Cinar, G., Mavris, D. N., Emeneth, M., Schneegans, A., & Fefermann, Y. (2017). Development of parametric power generation and distribution subsystem models at the conceptual aircraft design stage. In 55th AIAA Aerospace Sciences Meeting (p. 1182). DOI: 10.2514/6.2017-1182

Development of Parametric Power Generation and Distribution Subsystem Models at the Conceptual Aircraft Design Stage

Gokcin Cinar,* Dimitri N. Mavris,†
Aerospace Systems Design Laboratory, Atlanta, GA, 30332

Mathias Emeneth,‡ Alexander Schneegans§
PACE America Inc., Seattle, WA, 98115

Yann Fefermann,¶
Safran Tech, Magny-Les-Hameaux, 78772, France

The ongoing efforts to reduce aviation related greenhouse gas emissions and fuel burn have led to advancements in power generation and distribution (PG&D) subsystem technology. Due to the absence of historical data, PG&D subsystem models must be created from first-order analysis without compromising crucial information on their characteristics. This paper demonstrates the development of parametric, physics-based subsystem models such as battery, electric motor, power distribution and management system, and propeller speed reduction unit for rapid and low-cost sizing, simulation and analysis at early design stages. A special focus was put on rechargeable battery technology and implementing a dynamic (rather than steady-state) discharge behavior into the propulsion architecture. A methodology to integrate the developed subsystem models was presented. A sample application was also provided to demonstrate the combined capabilities of the models. To this end, the models were applied within a sample parallel hybrid electric architecture using Dornier 328 as a test bed. The subsystem behaviors under varying power requirements were then analyzed. Finally, the importance of having more dimensionality at the subsystem level at early design stages was highlighted by comparing the results of two different architectural choices.

I. Introduction

NOWADAYS, electric and hybrid electric propulsion technologies are in the spotlight as a response to the increasing demand for greener aviation. NASA N+3 goals (i.e. technologies nearing maturity in 2025) aim for more than 75% reduction in Landing Takeoff NO_x emissions and more than 70% reduction in aircraft fuel burn with new cutting-edge aircraft designs and technology improvements.[1,2] These potential designs include but not limited to Bauhaus Luftfahrt's fully electric Ce-Liner concept, Boeing's SUGAR parallel hybrid electric aircraft concepts and NASA's N3X blended wing body concept.[1,3–5] As it can be seen from these examples, the substantial change in the propulsion systems also brings new challenges to the aircraft design community. One particular and important but not yet thoroughly addressed challenge lies in the architecture design.

The electric and hybrid electric aircraft concepts pose a significant subsystem architecture challenge. The subsystems used in the electric propulsion system are responsible for providing the propulsive power.

*Graduate Researcher, School of Aerospace Engineering, Georgia Tech, AIAA Student Member
†S.P. Langley Distinguished Regents Professor and Director of ASDL, School of Aerospace Engineering, Georgia Tech, AIAA Fellow
‡Senior Business Development Manager, PACE America, AIAA Member
§President, PACE America, AIAA Member
¶System Architect, Energy and Propulsion Department, Safran Tech

Therefore, very large amounts of power propagates through these subsystems.[3] This creates a challenge especially in terms of generation and distribution of power. Apart from the subsystems themselves, the sizing of the distribution elements are also affected by the magnitude of the current which they carry, and hence might introduce significant amounts of weight to the system. As a result, there is a need to study these revolutionary concepts from a subsystems perspective.

Traditionally, the sizing of the subsystem components is performed during the conceptual aircraft design stage by using empirical relationships based on existing historical data.[6,7] From these empirical relations, information on aircraft weight, power (or thrust) and drag polar are then estimated and fed into the sizing and synthesis process where constraint analysis (to meet point performance requirements) and mission analysis (to fly a specific design mission) are carried out through iterations.[8] However, there is a lack of historical data and readily available physics-based models for unconventional or more recent technologies such as electric propulsion (EP) and hybrid electric propulsion (HEP) subsystems. Hence, estimations on the impact of PG&D subsystems add uncertainty to the system.

In previous work done by the authors, a methodology for evaluating subsystem level effects of electric propulsion technology on system level design metrics was proposed.[9] In order to perform more comprehensive analyses and obtain more accurate results, more detailed subsystem models must be used in this proposed methodology or other approaches which can be found on literature. Specifically, an accurate model for the battery package is vital to reflect its unsteady dynamics. However, it should also be kept in mind that the level of complexity of these models must be suitable for early design phase analyses. Hence, the trade-off between the accuracy and cost and/or complexity of the models must be considered carefully, especially for batteries due to their highly complex and specific electro-chemical structures.

Consequently, there is a need for moderately complex physics-based models for rapid, low-cost analysis to investigate the potentials and implementation strategies at early design stages. The objective of this work is to adapt and implement parametric rechargeable battery model which captures the dynamic charging and discharging behavior as steady-state behavior can yield misleading and inaccurate results. Compatible and parametric models for other essential PG&D subsystems such as a rubberized electric motor, power management and distribution unit, and propeller speed reduction unit will also be constructed. Finally, these components will be sized and applied within a sample propulsion architecture using Dornier 328 as the baseline aircraft. The analysis will be performed to reveal the interactions between the subsystems and the vehicle performance and their effects on each other in the conceptual design stage.

II. Overview of Electric Propulsion Subsystems

Figure 1 shows a notional power train for EP, HEP connected in parallel and HEP connected in series configurations where electrical energy is delivered from a battery to an electric motor. As it can be seen from Figure 1, the electrical energy travels through similar subsystem components in all three concepts; including but not limited to a battery as the primary or secondary energy source, a power converter for voltage and current conversions, an electric motor, generator, and transmission system.

In order to investigate the major subsystems' roles in EP/HEP architectures, their most prominent features and working principles will be studied first. Then, parametric models will be built up based on the findings of this study so that they could represent the actual characteristics accurately enough for conceptual design stage analyses.

The following sections give an overview on the mathematical approaches of the creation of the following PG&D subsystem models: battery, power converter, electric motor, power distribution and management unit, and propeller speed reduction unit.

A. Rechargeable Battery

1. *Introduction to Electric Battery Concept*

Battery cells convert chemical energy to electrical energy through electrochemical reactions and generate DC electricity. This is called a "discharge" process. Rechargeable battery cells can reverse this chemical reaction when current is sent into the battery. This is called a "charge" process.[10]

Although the terms "battery" and "cell" are sometimes used interchangeably, a battery is actually made up of at least two cells connected in series configuration. Each cell has a positive terminal (cathode) and a negative terminal (anode). When the positive terminal of a cell is connected with the negative terminal of

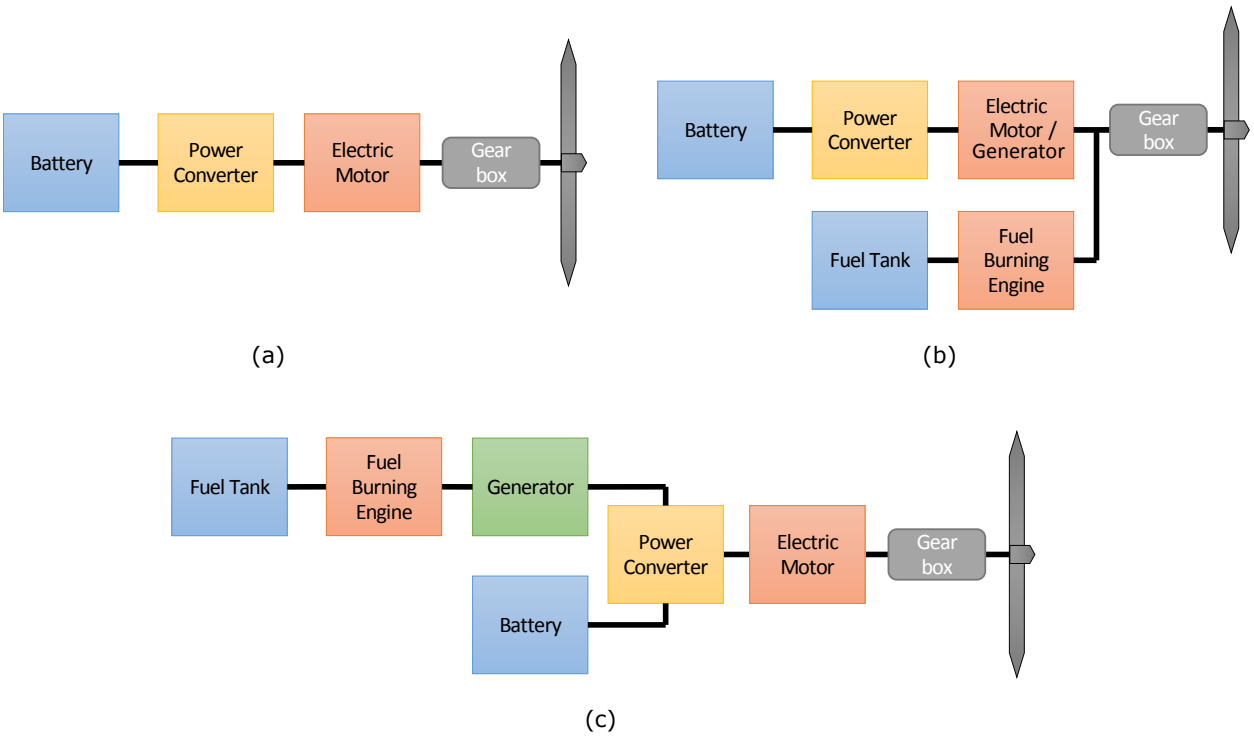

Figure 1. Notional subsystem components and architecture for (a) Electric propulsion, (b) Hybrid-electric propulsion connected in parallel, (c) Hybrid-electric propulsion connected in series

another cell, it is called a series connection. When the positive and negative terminals of a cell are connected with the positive and negative terminals of another cell respectively, it is called a parallel connection.

Battery voltage, current and energy analyses are usually performed by building equivalent circuit models. Such a sample model is demonstrated in Figure 2. Here, the battery is described by an internal resistance R and open-circuit voltage E, which is the electrical potential when no load is connected to the circuit. When a current i flows through the battery, power is dissipated by the internal resistance as heat and therefore the terminal voltage V is not equal to E. Eqn. 1 gives the mathematical description of this model.

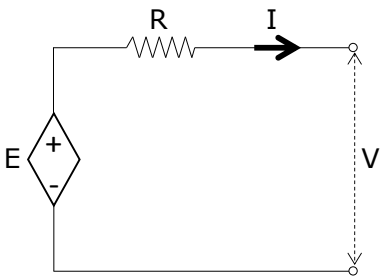

Figure 2. A simple equivalent circuit model of a battery[10]

$$\mathbf{V} = E - IR \tag{1}$$

Cells are connected in series and/or parallel in order to increase the voltage or charge capacity of the battery. When n number of cells are connected in series, then following Kirchhoff's voltage law, the total voltage of the battery is the sum of individual voltage values of each cell as given by Eqn. 2. Similarly, the sum of internal resistance of each cell gives the overall internal resistance of the battery as given by Eqn. 3.

$$E = \sum_{j=1}^{n} E_j \tag{2}$$

$$R = \sum_{j=1}^{n} R_j \tag{3}$$

In the case of m number of parallel cell connections, Kirchhoff's current law is followed by summing up the currents flowing through each cell to find current flowing through the battery (Eqn. 4); and the internal

resistance of the battery is given by equation Eqn. 5.

$$I = \sum_{j=1}^{m} I_j \tag{4}$$

$$R = (\sum_{j=1}^{m} \frac{1}{R_j})^{-1} \tag{5}$$

It should be noted again that the model shown in Figure 2 is a simplified one and is not suitable for the complexity of our analyses. In the upcoming sections, a more detailed model will be discussed.

2. General Parameters

Battery package is a very important component in electric and hybrid-electric vehicle applications as it is the main or secondary energy source and introduces significant weight to the system.[9] Hence, choosing the right type and size of the battery is vital for the overall design.

There are various types of rechargeable batteries such as lead acid, nickel metal hydride (NiMH), lithium polymer, etc. but their behavior and performance can be described as common parameters. These parameters will play an important role in developing the battery model. Therefore, it is deemed necessary to give a detailed description of these parameters below along with their respective SI units.[10]

- **Specific Energy [Wh/kg]:** The most obvious performance parameter that is directly related to the endurance of an aircraft is battery's specific energy. It is defined as the amount of electrical energy stored for unit battery mass.

- **Energy Density [Wh/m^3]:** Similar to specific energy, this is the amount of electrical energy stored for unit battery volume.

- **Specific Power [W/kg]:** This is the amount of power obtained per unit mass of the battery. A battery which has high specific power can take in and give out energy very rapidly and therefore would be very beneficial for aircraft operations that require relatively high power.

  In fact, technology comparisons between batteries are usually made by comparing their specific energy and specific power because there exists a strong trade-off between them. The capacity and energy efficiency of a battery decrease with shorter discharge time. As a result, during high power operations the battery capacity drops rapidly. Hence, if a battery has high specific energy, then it suffers from low specific power characteristics and vice versa.

- **Charge Capacity [Coulomb or Ah]:** Charge capacity, sometimes referred as charge or capacity, is the load current a battery can deliver over time. The higher charge capacity a battery has, the longer time it will run. Although the SI unit for capacity is coulomb, in battery technology Ah (ampere-hour or amphour) is a more widely used unit as it describes 1 ampere supplied for 1 hour which is more a more practical description for battery applications.

  The capacity can be given numerically as, for example, "15 Ah", or "C = 15 A". Both of these notations have the same meaning: that is, the battery can provide 15 A if it is discharged for 1 hour, or 3 A if discharged for 5 hours, or 1 A if discharged for 15 hours, etc. Hence, in accordance with common sense, the higher the discharge current is, the shorter the battery will last and vice versa.

  Battery manufacturers usually give a nominal charge capacity. Then, all other charging/discharging cases are usually based on the nominal capacity value. For example, let the nominal capacity be given as C = 20 A. Then, "discharging the battery at 40 A for half an hour" and "discharge current of 2C" (i.e. 2 times C equals 40 A current) have equivalent meanings.

  Although battery capacity is a vital parameter, it does not completely describes the actual discharging behavior in practice. Discharge time and capacity are not always linearly proportional. In fact, shorter discharge time has a negative effect on capacity due to unwanted side reactions. The longer the discharge time is, the more charge capacity the battery will have. Referring to the first example, for a battery with C = 15 A, if the discharge current is 1 A the battery will most probably last more than 15 hours; whereas if the the discharge current is 30 A it will last less than 30 minutes. Since discharge

time can have a significant effect on capacity, it is very important not to neglect these fluctuations with various current draws during flight.

To eliminate any possible confusion with C, the capacity will be given by the letter Q throughout the rest of this paper.

- **Stored Energy [Wh]:** The energy stored in the battery is expressed by Wh (instead of the SI energy unit of Joules because Wh is a more practical unit for battery applications). It is given by Eqn. 6:

$$\mathbf{E} = V * Q \tag{6}$$

where V is the battery voltage, and Q is the capacity in Ah. However, as mentioned previously, all of these terms depend on how quickly or slowly the battery is charged or discharged. Under a high current draw, i.e. a rapid discharge process, the battery would be out of its stored energy very quickly as both V and Q would drop, and vice versa.

- **State of Charge:** State of charge, or SOC, can be defined as the ratio of the remaining capacity to the nominal capacity. This parameter is also very important as it provides information on the potential run time of the battery. Mathematically 100% SOC means a fully charged battery and 0% SOC means a fully discharged battery. However, in some cases, batteries might be overly charged. Moreover, discharging a battery to 0% SOC can harm the battery permanently and therefore a minimum limit greater than 0% is set in practice. This limit is generally suggested to be 20% for most battery types except the lead acid one for which it is set to be 30%. Hence, when SOC hits this minimum limit, discharge process is stopped by the battery management system. The voltage value at which this limit is hit is called "the cutoff voltage".

- **Depth of Discharge:** Depth of discharge, or DOD is the ratio of the discharged capacity to the nominal capacity; also given by Eqn. 7:

$$\mathbf{DOD} = 1 - SOC \tag{7}$$

3. Charge and Discharge Characteristics

Battery manufacturers usually provide a discharge curve for each battery they sell such as depicted in Figure 3. This curve shows the discharge behavior under a certain current draw in terms of battery voltage and capacity (or sometimes discharge time). Figure 3 shows an imaginary Lithium-Ion (Li-Ion) type of battery discharge characteristics. These type of batteries usually have an exponential zone at the beginning of discharge, and then the discharge curves remain almost constant for a considerable amount of battery run time. Voltage starts to drop very rapidly somewhere around the cutoff voltage, and continues to drop even more as the battery is fully discharged. The nature of these curves depend on the battery type and properties. But the main idea behind these curves is that voltage drops as battery is discharged, and increases as battery is charged.

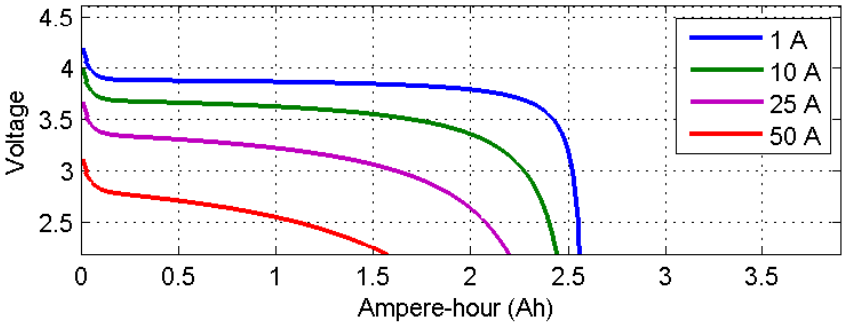

Figure 3. A sample discharge curve for a Lithium-Ion battery

This behavior is the main reason why the equivalent circuit model given by Figure 2 and Eqn. 1 cannot fully capture the discharge characteristics, as it assumes a constant battery voltage over time.

Furthermore, it can be seen from the different colored curves in Figure 3 that drawing a high amount of current (e.g. the red curve) over a short amount of time decreases the battery run time whereas drawing a low amount of current (e.g. the blue curve) over a longer time increases the run time, as described previously.

In many cases, charge characteristics can be assumed the same as discharge characteristics although they might not be exactly the same.[10]

4. Choosing a Suitable Battery Model

There are various models on battery dynamics in literature, however it is important to find a suitable one that matches the level of complexity of the intended application. The objective of this work is to implement low-cost models that would yield reliable results for conceptual design stage. Therefore, the simple open circuit model given by Figure 2 and Eqn. 1 would lead to loss of critical information on the dynamic behavior of the battery.

On the other hand, a very detailed model might give results that are close to reality at the expense of a high computational cost. Since the conceptual aircraft design stage is a phase where the designer would like to analyze the impact of changing parameters on the whole vehicle design by running numerous cases, such a model could easily become impractical. Furthermore, it must be taken into account that the conceptual designer is not necessarily an expert on each of the subsystems and therefore the models should be moderately easy to use.

One approach for battery modeling is to use empirical data and create fitting equations via regression techniques. Such empirical models give computational advantage and could also produce accurate results to some extent.[11] However, generally this accuracy is limited to certain operating conditions. Hence, these models fail to project the future technology improvements. Since this work aims to implement flexible models that can also be used in "what-if" kind of scenarios, employing empirical models would not be a suitable approach.

Another type is electrochemical models which incorporate chemical and electrochemical kinetics and transport phenomena.[12,13] There are a number of different approaches in this type of modeling and most of them produce more accurate results than empirical models. Employment of the physicochemical principles also allows the design of new battery chemistry or materials. However, the usage of such a model would require tremendous amount of expertise and would also be computationally costly. Thus, this type of models would not be suitable for the scope of this work either.

Equivalent circuit models can produce accurate results without going into battery chemistry provided that the model is properly built up to reflect battery characteristics. Although the equivalent circuit model shown in Figure 2 is a simple one, it can be improved by adding extra circuit components.[14] Hence, a trade-off can be done between the complexity and accuracy to fit the model to a specific application. One such model, presented by Tremblay and Dessaint[15] was deemed reasonable to fulfill the purpose of this work in terms of its easiness of use and level of detail. Here, we shall give a brief summary of this model and quote a set of equations specifically for Li-Ion type of battery, but the interested reader can refer to Ref.[15] for further details and other battery types.

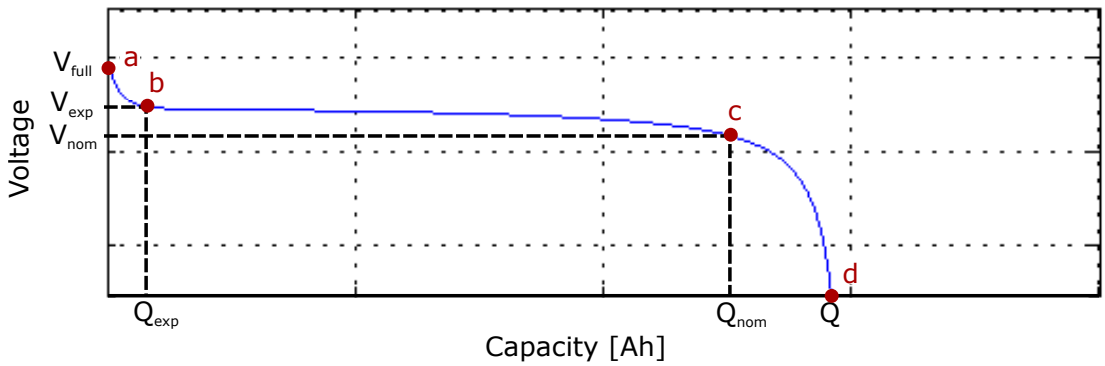

Figure 4. A sample discharge curve for a Lithium-Ion battery

Tremblay and Dessaint's model[15] takes two special points along with the extremes on a typical discharge characteristics curve given at a constant current to predict the battery behavior at any other current using a set of equations. The extremes are the fully charged voltage V_{full} (point a) and the maximum capacity Q (point d). The remaining two points are namely "the end of the exponential zone" and "the end of the nominal zone" which are given by points b (Q_{exp}, V_{exp}) and c (Q_{nom}, V_{nom}) in Figure 4, respectively. "The end of the exponential zone" is the point at which the curve ends its exponential behavior at the beginning of discharge, whereas "the end of the nominal zone" is the point at which the voltage starts to drop abruptly. The model also use the internal resistance (R).

The discharge and charge voltages as a function of capacity for Li-Ion type of batteries are given by Eqn. 8 and Eqn. 9, respectively.

$$\mathbf{V_{batt} = E_0 - RI - K\frac{Q}{Q - Q_{act}}(Q_{act} + I^*) + A\exp(-B * Q_{exp})} \tag{8}$$

$$\mathbf{V_{batt} = E_0 - RI - K\frac{Q}{Q_{act} - 0.1Q}I^* - K\frac{Q}{Q - Q_{act}}Q_{act} + A\exp(-B * Q_{exp})} \tag{9}$$

where V_{batt} is battery voltage [V] , E_0 is battery constant voltage [V], Q_{act} is actual battery charge [Ah], and I^* is filtered current [A]. The terms K (polarization constant [V/Ah] or polarization resistance [Ω]), A (exponential zone amplitude [V]) and B (exponential zone time constant inverse [$(Ah)^{-1}$] are calculated using the previously chosen points on the typical discharge curve and Equations 10, 11 and 12 as follows:

$$\mathbf{K = \frac{-E_{nom} + E_0 + A\exp(-BQ_{nom})(Q - Q_{nom})}{Q(Q_{nom} + I)}} \tag{10}$$

$$\mathbf{A = E_{full} + E_{exp}} \tag{11}$$

$$\mathbf{B = \frac{3}{Q_{exp}}} \tag{12}$$

In this model, the internal resistance R is assumed to remain constant all the time. Moreover, temperature effects and self-discharge of the battery are neglected. Finally, the battery capacity is assumed to be independent of the current amplitude.

B. Power Converter

In the previous section, we explained how battery voltage changes as the battery is charged or discharged during flight. However, the battery supplies energy to the electric motor or other non-propulsive subsystems which might work under different voltage demand. Therefore, a nominal system voltage must be set independent of the battery voltage to keep consistency between other subsystem voltage requirements.

A power converter converts electrical power by changing input voltage to a desired output voltage.[16] Eqns. 13, 14 and 15 show this conversion, where η_{pc} is the efficiency of the power converter.

$$\mathbf{P_{pc,in} = I_{pc,in}V_{pc,in}} \tag{13}$$

$$\mathbf{P_{pc,out} = I_{pc,out}V_{pc,out}} \tag{14}$$

$$\mathbf{P_{pc,in} = \frac{P_{pc,out}}{\eta_{pc}}} \tag{15}$$

C. Electric Motor

1. *Introduction and General Parameters*

Electric motors convert electrical power to mechanical (shaft) power. They can operate at very high efficiency and have high reliability. Electric motor efficiency is independent of operational altitude which gives an advantage over conventional internal combustion engines.[10] Furthermore, recent advances in electric motors

enabled higher power-to-weight ratios (i.e. specific power), such as Siemens' electric motor for aircraft which has a state-of-the-art power-to-weight ratio of 5 kW/kg and delivers a continuous output of about 260 kW.[17]

Performance of an electric motor is determined by its torque (T) and rotational speed (ω) characteristics. Shaft power (P_{mech}) is calculated using Eqn. 16, whereas electric power (P_{el}) is given by Eqn. 17. An ideal electric motor would convert electrical power into mechanical power with 100% efficiency, and therefore the two expressions in Equations 16 and 17 would be equal to each other. However, real life motors suffer from losses due to some magnetic effects, heat dissipation caused by friction, etc. Hence, it is more realistic to make the connection between electrical (input) power and mechanical (output) power via an efficiency factor as shown in Eqn.18, where η_{EM} is the electric motor efficiency.

$$\mathbf{P_{mech} = T\omega_{EM}} \tag{16}$$

$$\mathbf{P_{el} = I_{EM}V_{EM}} \tag{17}$$

$$\eta_{\mathbf{EM}} = \frac{\mathbf{P_{mech}}}{\mathbf{P_{el}}} \tag{18}$$

There are mainly two types of electric motors which are mostly used in electric vehicles: brushed DC motors and brushless motors. Brushed DC motors are widely used as traction motors in electric cars. These types of motors are easier to control. Torque of a brushed DC motor is directly proportional to the current traveling through its wires (also known as rotor or armature current). This relation is given by 19 where k_T is the torque constant in [Nm/A] and I_A is the armature current in [A]. Value of the torque constant depends on the motor design.

$$\mathbf{T = k_T I_A} \tag{19}$$

In case the torque-current relationship of a motor is more complex or completely unknown, current going into the motor can still be found by Eqn. 19 to simplify the calculations. Moreover, it can be seen by comparing Equations 16, 17, 18 and 19 that a similar relationship also exists between the motor speed and voltage as well.

2. Loss-based Electric Motor Model

Inefficiencies in an electric motor can be caused by various factors depending on the motor design, torque and speed. If these losses can be calculated, then the motor efficiency for different operation conditions can be approximated and an efficiency map can be created. Efficiency maps consist of efficiency islands for each allowable torque-speed combination and are useful to determine the optimum torque and speed settings.

In order to develop an electric motor model, the major sources of loss must first be identified. Lowry and Larminie[10] divides the major sources of loss into four main sections which are generally the same in all motor types, as follows:

- **Copper Losses:** caused by energy dissipation into heating due to the electrical resistance of wires. It is proportional to the second power of armature current and therefore to the torque as shown in Eqn. 20 where k_c is a constant that depends on brush resistance and magnetic flux. This type of loss can be the largest cause of inefficiency especially for small motors.

$$\mathbf{Copper\ Loss = k_c T^2} \tag{20}$$

- **Iron Losses:** caused by the ever-changing magnetic field effects in the iron of the motor. It is proportional to motor speed as given by Eqn. 21 where k_i changes with variations in the magnetic field strength but can be assumed constant.

$$\mathbf{Iron\ Loss = k_i \omega_{EM}} \tag{21}$$

- **Friction and Windage Losses:** caused by a friction torque in the bearings of the motor and the wind resistance. Relevant power terms for friction and windage losses are given respectively in Eqn. 22 and Eqn. 23, where T_f is the friction torque and k_ω is a constant which depends on the size and shape of the motor and whether it has a cooling fan.

$$\mathbf{Friction\ Power} = \mathbf{T_f \omega_{EM}} \tag{22}$$

$$\mathbf{Windage\ Power} = \mathbf{k_w \omega_{EM}^3} \tag{23}$$

- **Other Losses:** occurs regardless of the torque and speed of the motor, even when the motor is stationary. It is shown with the letter C.

The total loss is given as the sum of all these losses as shown in Eqn. 24 and can be assumed true for all motor types.

$$\mathbf{Total\ Losses} = \mathbf{k_c T^2 + k_i \omega_{EM} + k_w \omega_{EM}^3 + C} \tag{24}$$

Since the efficiency is given by the ratio of output power to the input power (which is the output power combined with total losses), efficiency η_{EM} can be calculated by Eqn. 25.

$$\eta_{\mathbf{EM}} = \frac{\mathbf{T \omega_{EM}}}{\mathbf{T \omega_{EM} + k_c T^2 + k_i \omega_{EM} + k_w + C}} \tag{25}$$

The constants given in these equations can be found based on experimentation or regression.

A comparison between Eqn. 18 and 25 gives the electrical power P_el in terms of the motor losses as given in Eqn 26. If the loss constants and operating conditions are known in terms of motor torque and rotational speed, then supply voltage and current can easily be calculated using equations 19 and 26.

$$\mathbf{P_{el}} = \mathbf{T \omega_{EM} + k_c T^2 + k_i \omega_{EM} + k_w} \tag{26}$$

3. Power Management and Distribution (PMAD)

PMAD is used to regulate the voltage according to the electric motor power requirements, as voltage variations from low to high values are usually necessary to control the speed of the motor.[18] PMAD can be modeled as a separate subsystem in detail, but for the scope of this work it will be treated as a power converter embedded into the electric motor model with its own separate efficiency. When it is desired to control the motor speed, PMAD converts the system voltage into the motor supply voltage and hence the motor speed changes according to the equations given above.

D. Propeller Speed Reduction Unit (PSRU)

PSRU is a gearbox which transfers the rotational motion of the motor output shaft to the propeller via a speed reduction.[19] Electric motors run at higher efficiency at higher rotational speeds relative to propellers which are more efficient at lower speeds due to tip speed and structural restrictions. Therefore, unless the electric motor is a direct drive motor, a PSRU is necessary to get the highest efficiency from both the motor and the propeller.

PSRU can be modeled by defining the relationship between the electric motor rotational speed (ω_{EM}) and the propeller rotational speed (ω_{prop}) through a predefined gearbox ratio (R_g) as given in Eqn. 27. The input power is calculated from Eqn. 28 where η_{PSRU} is the efficiency of the PSRU.

$$\mathbf{R_g} = \frac{\omega_{\mathbf{EM}}}{\omega_{\mathbf{prop}}} \tag{27}$$

$$\mathbf{P_{PSRU,in}} = \frac{\mathbf{P_{PSRU,out}}}{\eta_{\mathbf{PSRU}}} \tag{28}$$

III. Development of the Subsystem Models

The next step after defining the important parameters of each subsystem is to create compatible models out of these parameters and integrate them altogether within an hybrid electric architecture. To this end, the modeling and simulation environment was chosen to be Pacelab SysArc which is a system architecture design tool as part of a fully-fledged preliminary aircraft design environment. It allows to build, analyze and optimize system and subsystem architectures while instantly assessing their impact on the overall vehicles performance. It comes with an extensive library of different system components such as generators, motors, pumps, batteries, power converters etc., it creates automatically connecting distribution elements such as cables, pipes, ducts etc. and allows the application of different flight and failure modes on the architecture.

The aforementioned subsystems will be constructed as Engineering Objects (EO) within SysArc's Knowledge Designer, which is a sandbox where components can be characterized mathematically and defined geometrically. Once EOs are created, these building blocks become available to a component library which is used in the end-user application, Pacelab SysArc Engineering Workbench, to create the system models and analyze architectures.

Each EO created in Pacelab SysArc has an input and/or an output port so that when two EOs are "logically connected", information can pass through from one component to another. Logical connections are allowed only if components are compatible with each other.

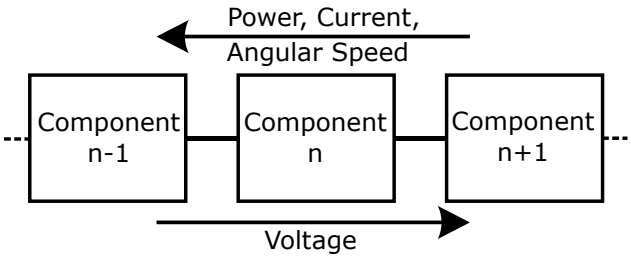

Figure 5. Direction of information propagation between subsystem component ports

Figure 5 demonstrates the direction of information propagation between logically connected components and the types of port parameters. Power, current and angular speed are propagated upstream (i.e. from an output port to an input port) whereas voltage is propagated downstream (i.e. from an input port to an output port). For example, if the output port of *component (n-1)* and input port of *component n* are electrical ports, then once connected, the output power and current of *component (n-1)* will be supplied by the input power and current of *component n*. In contrast, the input voltage of *component n* will be supplied by the output voltage of *component (n-1)*.

The following sections will explain how the power generation and distribution subsystems were constructed within Pacelab SysArc.

A. Battery Model

1. *Calculating the State of Charge*

It has been discussed in detail in Section II.A that the performance of the battery has a vital impact on the overall performance of the flight due to the continuously changing discharge behavior under different power needs. Hence, it is important to have control over the battery run time at each point of the flight. This can be done by checking the battery SOC at certain time steps throughout the mission.

In the case of a discharge process, the battery will try to match the power requirement by changing the amount of current. To do so, it has to have enough capacity throughout a time interval in which the power demand is assumed to be constant (i.e. time interval between two successive mission legs). The battery SOC at the end of a mission leg is then calculated by the power drawn out of the battery for a given time interval. A battery control management system can check whether the SOC value at the end of each mission leg is above a minimum limit. If SOC hits a certain limit the discharge process is immediately terminated.

As a result, the battery model implemented into Pacelab SysArc relies on SOC checks at predefined time intervals. These time intervals may vary throughout the flight. For example, during the flight segments in which power requirement can change drastically (e.g. during takeoff, climb, etc.), a rather short time interval should be set to reflect an accurate battery discharge behavior. In the segments where the power requirement follows a more or less uniform pattern (e.g. cruise), the time intervals can be kept longer in order to ease the computational burden. Hence, a time interval must be strategically defined throughout the mission.

The SOC at the end of each time interval dt is calculated as follows: For each dt time, the amount of current that the battery delivers is given by the actual charge capacity Q_{act} as given in Eqn. 29.

$$\mathbf{Q_{act}} = I_{disch} * dt \tag{29}$$

Then, the battery voltage V_{batt} can be calculated for each time interval dt using equations 8 through 12. Finally, the capacity left in the battery is determined, and the final SOC can be calculated by Eqn. 30.

$$\mathbf{SOC_f} = SOC_i - \frac{\sum Q_{act}}{Q} * SOC_i \tag{30}$$

Finally, this SOC_f value is checked to see whether it is above the pre-specified minimum SOC limit. If it is, then the final battery voltage after the discharge process is calculated, and SOC_i value is updated by the SOC_f value before moving to the next time interval. The battery voltage is also reported and propagated upstream so that the other subsystem components connected directly to the battery are informed. In the case that SOC drops under the minimum limit, the discharge process must be terminated.

2. The User Interface of the Model

In Pacelab SysArc, the user can interact with the input and output parameters of the mathematical model through an interface called "Properties View" which is unique to each model. A screen-shot from the "Properties View" for the battery is shown in Figure 6.

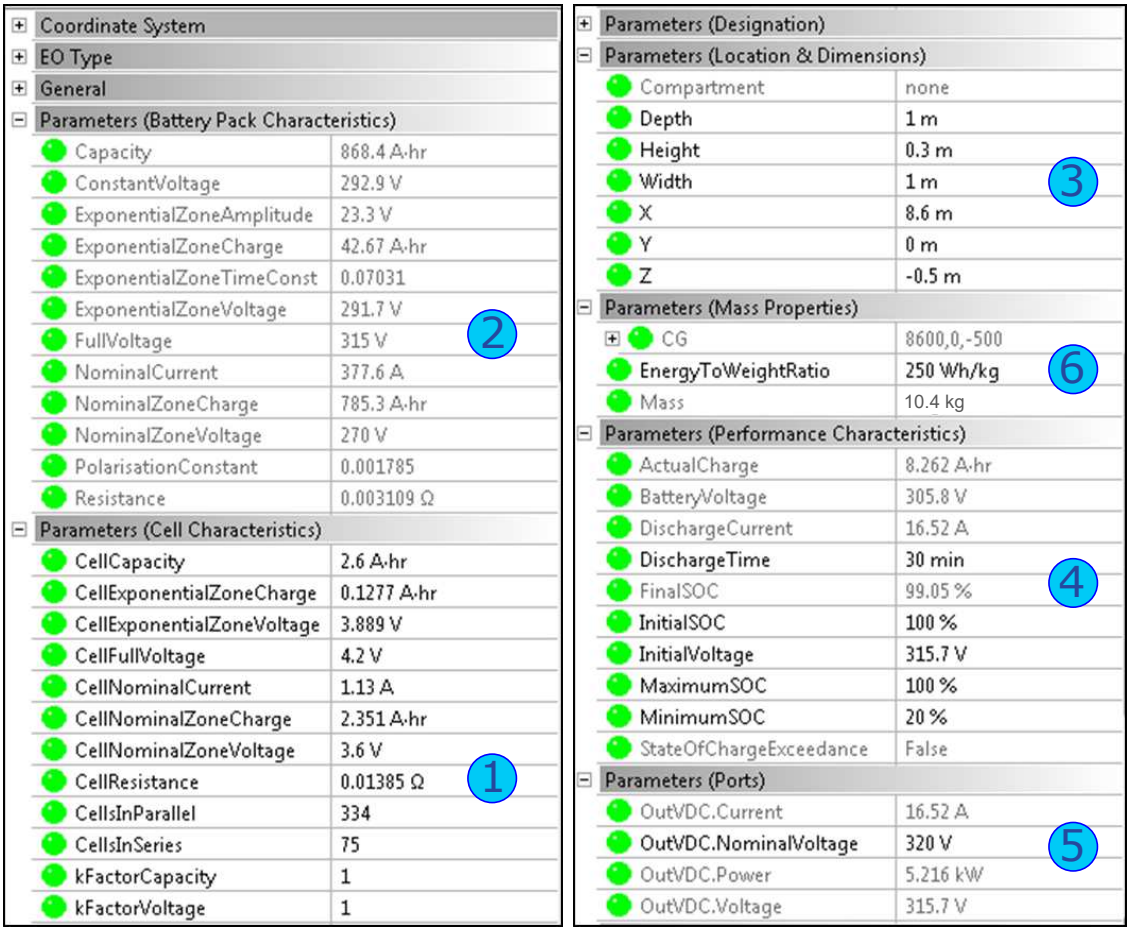

Figure 6. "Properties View" of the adapted battery model in Pacelab SysArc

The parametric battery model is divided into 5 main parts as seen in Figure 6. These parts are explained as follows:

1. **Cell Characteristics:** The user first specifies the cell level characteristics. Capacity, voltage, resistance and nominal current values can be found from manufacturer's data sheet, as explained in Section II.A.4. The user is then asked to determine number of cells connected in parallel and series to build a battery out of these cell characteristics. The two parameters at the bottom are technology k-factors for cell capacity and voltage which will be explained in further detail in the upcoming section.

2. **Battery Pack Characteristics:** Once the cell characteristics are fed into the model, it calculates similar characteristics at the battery level. The voltage and current values are calculated according to Kirchhoff's laws as previously described in Section II.A.1. The model assumes that the battery efficiency is equal to the cell efficiency, voltage or charge related losses are ignored while building up the battery from cell characteristics.

3. **Location & Dimension:** The physical location and dimensions of the battery inside the aircraft are defined here.

4. **Performance Characteristics:** In this model, the aforementioned time interval between each mission leg is given by "Discharge Time". For steady-state calculations, the user can manually set a single discharge time to calculate the final state of the battery. For transient calculations, i.e. while aircraft is flying a given mission profile, this time interval is automatically determined by the time between two successive mission legs, as well as the final SOC at the end of each mission leg.

5. **Ports:** Here, the parameters are automatically propagated to/from connected subsystems.

6. **Mass Properties:** Overall electrical energy drawn out of the battery is calculated by the discharge times and power values outside of the Properties View. The user specifies battery's "energy-to-weight-ratio" (i.e. specific energy) and the weight of the battery calculated from this ratio and the overall energy. In this sense, the weight of the battery is independent of the number of cells.

   It should also be noted that Pacelab SysArc allows the user to toggle the input and output parameters provided that they are mathematically related. Therefore, if either of the input or output current value is known, then their input-output position can be swapped.

3. The Model Flexibility

The parametric nature of the model allows creating non-existing or distinctive characteristics and studying individual and/or combined effects of each variable. Although a manufacturer's data sheet may be enough to simulate an existing battery behavior, the model can also be used to estimate the impact of technology advancements.

The technology trends show that future cells will evolve to have higher specific energies.[20] Therefore many electric aircraft studies look only at specific energy while doing technology sensitivity analyses. However, more dimensions at subsystem level must be comprised to explore and evaluate candidate architectures. For example, an architecture study would be incomplete if the maximum amount of current which flows through the cables is unknown. Hence, it is important to estimate voltage and capacity advances that will eventually lead to improvements in specific energy.

Looking back at Figure 3, it can be seen that the battery model uses four specific points to estimate the rest of the discharge curve. Leveraging this feature of the model, the authors would like to take it a step further and introduce a new capability for technology projection purposes by independently and intelligently moving these points in space to investigate promising options.

New discharge curves can be constructed by relocating these voltage and capacity points. To simulate an improvement in terms of voltage, the voltage values at points a, b and c can be increased whereas an improvement in terms of charge capacity can be modeled by increasing capacity values at points b, c and d. In the SysArc battery model, the user can alter these points at different amplitudes.

Figure 7 demonstrates various sample cases corresponding to such changes. The baseline cell and battery characteristics (Case 1) is shown by the blue curves in the discharge characteristics plots. If all the voltage values are doubled at the cell level, then the discharge curve extends upwards as given by the green curve (Case 2). On the other hand, if all the capacity values are doubled at the cell level, then the curve stretches to the right as given by the orange dashed curve (Case 3). Finally, Case 4 shows the combined effects of doubling both voltage and capacity. The changes at the cell level are translated automatically into the battery level by the model.

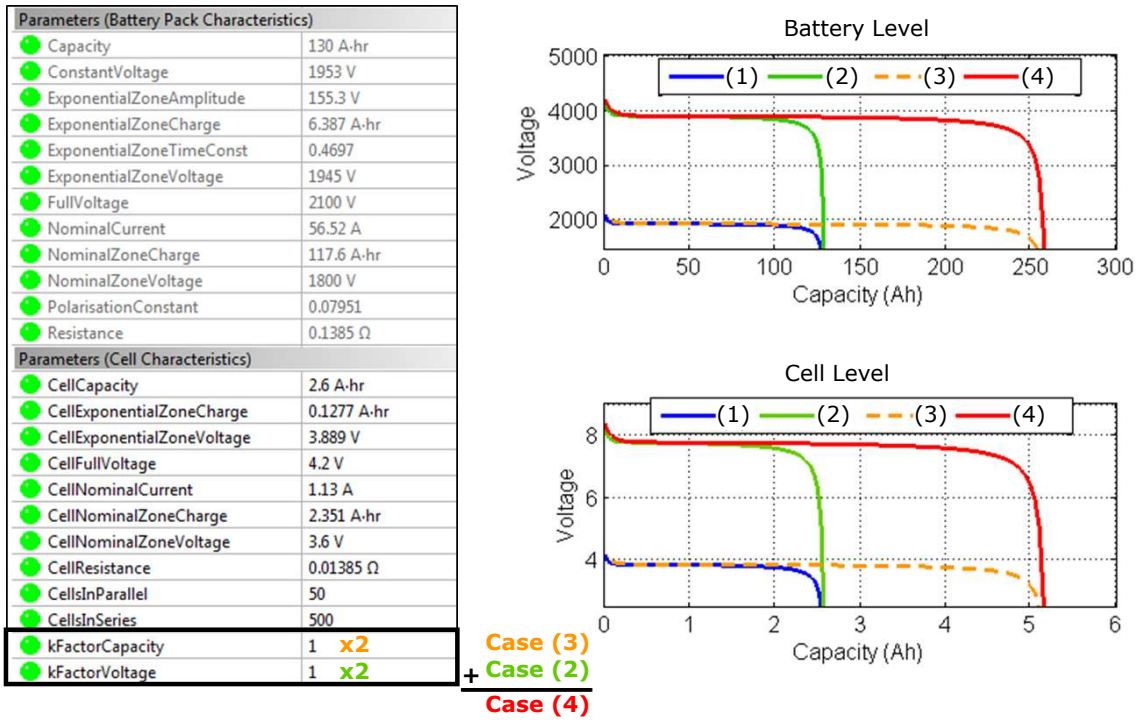

Figure 7. Various technology improvements at the cell and battery levels

Remembering that the stored energy is given by Eqn. 6, it can be easily seen that doubling both voltage and capacity increases energy by a factor of 4. Assuming the weight of the battery has been kept constant, specific energy also increases by a factor of 4. Scientists predict that today's state of the art batteries with 250Wh/kg of specific energy will reach to this level at the year 2020.[20]

While it is possible to play with each of the voltage (or capacity) points separately (especially to demonstrate distinct battery behaviors), it might make more sense to mimic the discharge behavior of the baseline battery type to perform technology projections on it. To simplify the afford for such technology projection studies, technology k-factors were added to the "Properties View" as it can be seen in Figure 7. In this example, doubling the voltage values at all three points corresponds to doubling k-factor for voltage which results in the green discharge curve (Case 2). Similarly, Case 3 can be obtained by doubling only the k-factor for capacity.

To summarize, the adapted mathematical model enables flexibility to represent different battery types or technology levels. The effect of such differences or improvements can then be tracked at the aircraft and mission levels. Moreover, this capability enables translating aircraft and mission requirements into battery characteristics without going into electrochemical simulations. This top-down approach would also be beneficial for scientists to set technology improvement targets.

B. Power Converter Model

The power converter model takes an input voltage along with a user defined efficiency and converts it to a desired output voltage as shown previously in Eqn. 13. The input power or required output power must also be known to perform the conversion. Power-to-weight ratio of the converter is an input to the the model and the weight of the component is calculated from this ratio and nominal power of the converter.

The input and output parameters of the model are listed in Table 1. The reader should not confuse the terms "input/output variables" given in two columns of Table 1 with the "input/output port" parameters. The parameters seen on the input column must be filled by the user so that the model can calculate the parameters on the output column. However, if two components are connected to each other, then the port parameters are automatically propagated as explained previously, and hence the user cannot alter them.

Table 1. Model input and output parameters of the Power Converter

Inputs			*Outputs*		
Parameter	Units	Description	Parameter	Units	Description
V_{out}	[V]	Voltage at the output terminal	I_{in}	[A]	Current going in
η_{pc}	%	Component efficiency	W_{pc}	[kg]	Component weight
P/W	[kW/kg]	Power to weight ratio			
P_{nom}	[kW]	Nominal power			
V_{out}	[V]	Voltage at the output terminal			
V_{in}	[V]	Voltage at the input terminal*			
I_{out}	[A]	Current going out*			

Such input port parameters which take their values from another component are designated with a "*" sign at the end of parameter descriptions. The rest of the input and output parameters can be toggled as long as the mathematical relations remain well-constrained.

C. Electric Motor Model

The loss-based model explained in Section II.C. (equations 16 through 26) together with the PMAD model was implemented into Pacelab SysArc as a single EO. Inputs and outputs of this combined model are tabulated in Table 2. Similar to the previous component, input port parameters designated with an "*" sign are propagated from the output port parameters of another component when connected. Furthermore, motor weight is calculated from power-to-weight ratio and rated power of the electric motor.

Table 2. Model input and output parameters of the Electric Motor with embedded PMAD

Inputs			*Outputs*		
Parameter	Units	Description	Parameter	Units	Description
$(P/W)_{EM}$	[kW/kg]	Motor P/W ratio	W_{EM}	[kg]	Motor weight
$P_{rated,EM}$	[kW]	Motor rated power	T	[Nm]	Motor torque
ω_{EM}	[rad/s]	Motor speed*	Iron Loss	[kW]	Iron Losses
P_{mech}	[kW]	Mechanical power*	Copper loss	[kW]	Copper losses
k_i	[Nm]	Iron loss constant	Windage loss	[kW]	Windage losses
k_c	[rad/s $(Nm)^{-1}$]	Copper loss constant	*Total Loss*	[kW]	Total power loss
k_w	[Nm $(rad/s)^{-2}$]	Windage loss constant	η_{EM}	%	Motor efficiency
C	[Nm/s]	Other loss constant	P_{el}	[kW]	Electrical power
k_T	[Nm/A]	Torque constant	$I_{in,EM}$	[A]	Motor current
η_{PMAD}	%	PMAD efficiency	$V_{in,EM}$	[V]	Motor voltage
$(P/W)_{PMAD}$	[kW/kg]	PMAD P/W ratio	$P_{PMAD,in}$	[kW]	Power into PMAD
$P_{rated,PMAD}$	[kW]	PMAD rated power	$I_{in,PMAD}$	[A]	Incoming PMAD current
$V_{in,PMAD}$	[V]	PMAD Voltage*	W_{pc}	[kg]	PMAD weight

D. PSRU Model

This component was modeled as given by Eqn. 27 and the input and output parameters can be seen in Table 3. Mechanical power at the output port (transmitted from the propeller) is scaled by the component efficiency and propagated to upstream (to the electric motor).

Table 3. Model input and output parameters of the PSRU

Inputs			*Outputs*		
Parameter	Units	Description	Parameter	Units	Description
P/W	[kW/kg]	Power to weight ratio	W_{pc}	[kg]	Component weight
P_{nom}	[kW]	Nominal power	ω_{EM}	[rad/s]	Motor speed
R_g		Gear ratio	P_{in}	[kW]	Input power
η_{PSRU}	%	Component efficiency			
P_{out}	[kW]	Output power*			
ω_{prop}	[rad/s]	Propeller speed*			

IV. Integration of the Subsystem Models

The developed models can be connected to each other through their port parameters as discussed previously. The direction of the parameter propagation was shown in Figure 5. A more detailed description is given in Figure 8 along with the corresponding port parameters for each subsystem.

The arrows denote the direction of the propagation, meaning that when a parameter is shown at the direction of the arrow, then it is fed by the port parameter of the neighboring subsystem. For example, in Figure 8, although $P_{batt,out}$ is an output parameter for the battery, it takes its value from $P_{PC,in}$ when connected with the power converter. The equal sign between the subsystems hold true if and only if there are no losses between the distribution elements (e.g. electrical cables). Otherwise, the losses must be added in the direction of the arrows.

The remaining port parameters are calculated as follows:

- V_{batt} from Eqns. 8 through 12
- $P_{pc,in}$ from Eqn. 15; $I_{pc,in}$ from Eqn. 13 (remember that $V_in, pmad$ is a constant input)
- $P_{pmad,in}$ same equations as the power converter with corresponding power, efficiency and voltage values for PMAD
- T from Eqn. 16; I_{EM} (same as I_A in this context) from Eqn. 19; P_{el} from Eqn. 26; and V_{EM} from Eqn. 17
- $P_{PSRU,in}$ from Eqn. 28; ω_{in} from Eqn. 27 (where ω_{out} is ω_{prop} when connected.

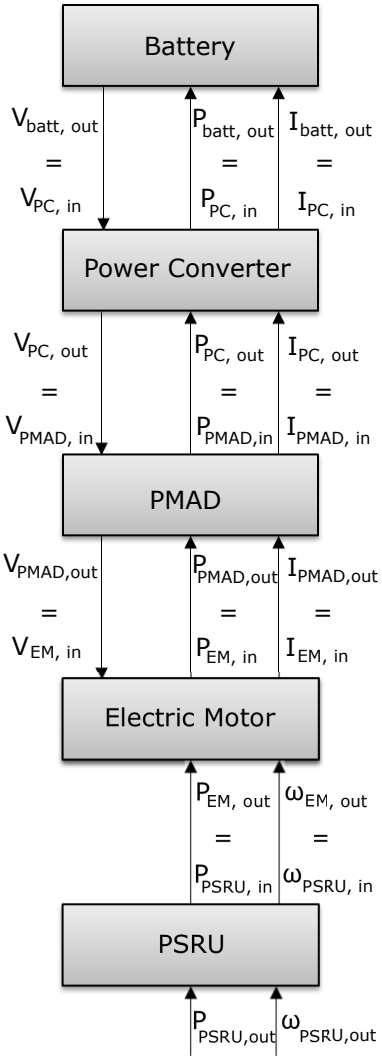

Figure 8. Propagation of the port parameters

V. Sample Application

The developed models can be used in many simulations and applications, including but not limited to sensitivity analysis, trade-off studies, architecture design space exploration, architecture comparisons etc. In this section, an example application will be provided to demonstrate the model capabilities in a use case scenario. The interested reader is referred to Cinar et al.[21] for further hybrid-electric applications and sensitivity analysis.

In the following paragraphs, the models will be applied within a baseline aircraft to build a parallel hybrid-electric propulsion architecture. Then, the PG&D subsystem responses will be analyzed under varying power requirements and architecture decisions.

A. Building Up the Subsystem Architecture in Pacelab SysArc

In this example, a parallel hybrid electric propulsion architecture was applied within a baseline aircraft. This baseline aircraft was chosen to be the Dornier 328, a regional turboprop commuter plane.[22]

Figure 9 illustrates the electric branch of the propulsion architecture. As it can be seen from this figure, there are two electric motors connected to each propeller in parallel and fed by a single battery pack and power converter. The system voltage was set to be 270 V. Moreover, a sample secondary subsystem per motor was also connected via generators. These secondary subsystems are generic electric loads running at a different voltage (230 V, AC). They represent a generic power off-take with varying power requirements throughout a flight segment.

First, the subsystems shown in Figure 9 were logically connected. The logical connections in Pacelab SysArc make sure the port parameters are propagated from one subsystem to another as described previously. Only subsystems with compatible ports can be connected. For example, if two subsystems run at different voltages, then a connection between them is not allowed by the tool unless there is a converter in between.

The next step after the logical connections were made is to replace the subsystems inside the baseline aircraft model in Pacelab and physically connect the components. Then, the automatic routing of the physical system connections were triggered. The logical connections automatically translate into physical connections (e.g. electrical wires) by the tool's routing algorithm which seeks the shortest possible route between two system components along the previously defined pathways. The wire weights are then computed based on the current passing through the wires and selection of wire type. Figure 10 depicts Dornier 328 with the PG&D subsystems right after the routing algorithm was performed. The electrical cables are shown in bold red.

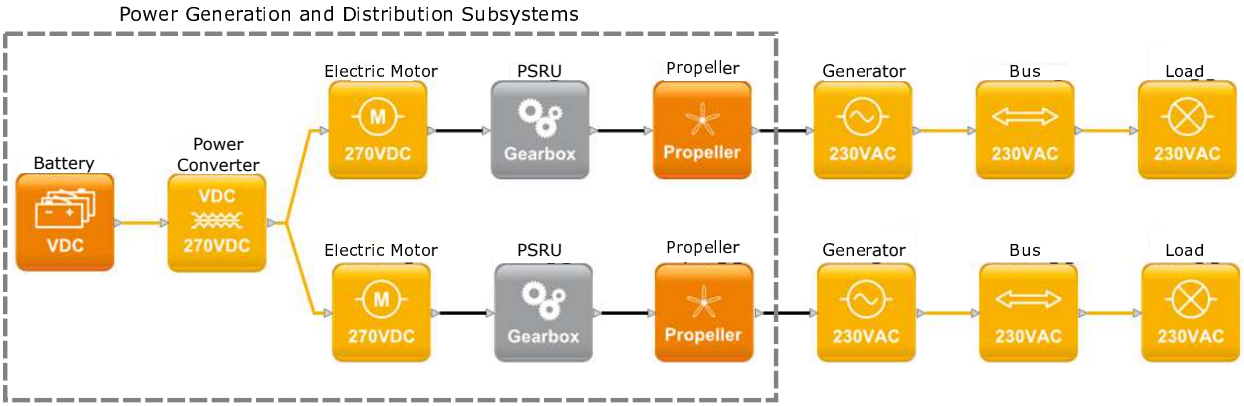

Figure 9. PG&D subsystems in a parallel hybrid electric architecture

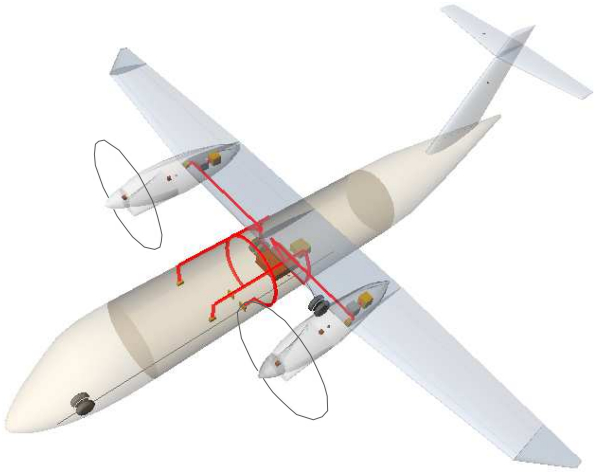

Figure 10. 3D drawing of the baseline aircraft in Pacelab SysArc

It must be noted that all the subsystems and the electrical loads were placed rather arbitrarily for demonstration purposes in Figure 10. Also, the turboprops were not shown in the hybrid electric architecture given in Figure 9, but can be seen in Figure 10.

B. Setting Up the Subsystem Characteristics

Aircraft required power varies throughout the flight not only due to changing flight conditions but also different needs of power off-takes. In order to analyze the subsystem responses under varying power requirements, an example scenario was set to represent a hypothetical flight segment. According to this scenario, it is assumed that all of the propulsive power requirement is provided solely by the turboprop engines of the baseline aircraft, whereas the two electrical loads are powered solely by the electric motors.

There are two secondary subsystems drawing power from the battery pack in the architecture shown in Figure 9. They are connected to the main PG&D architecture via two 230 VAC generators and buses; and their nominal powers were set to 100 kW each. During the 1-hour long hypothetical flight segment, each of the secondary subsystems operated at three different power levels (high, medium and low) according to the scheme shown in Figure 11.

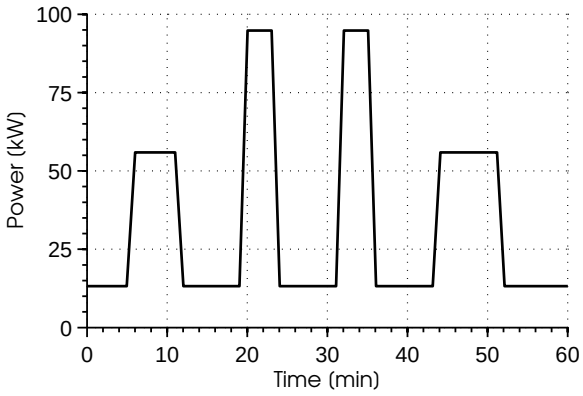

Figure 11. The low, medium and high power settings of each secondary subsystem varying through time

A state-of-the-art lithium-ion battery was was built up from the cell characteristics shown in Figure 6, with a cell capacity of 2.6 Ah and cell full voltage of 4.2 V. The battery was sized such that at the end of the 1-hour long flight segment, the SOC hits the minimum limit of 20%. This resulted in a battery consisting of 75 cells connected in series and 100 cells connected in parallel. The power converter, PMAD and PSRU efficiencies were set to a constant value of 95%. The electric motor characteristics are listed in Table 4.

Table 4. Electric motor characteristics

	Value	Units
k_T	0.35	[Nm/A]
k_i	0.1	[Nm]
k_c	0.08	[rad/s $(Nm)^{-1}$]
k_w	10^{-5}	[Nm $(rad/s)^{-2}$]

C. Results

Figure 12 shows the PG&D subsystem responses in terms of input and output port power, current and voltage values throughout the given 1-hour power-off take schedule. As explained previously and shown in Figure 8, the output parameter of a subsystem was assumed to be equal to the input parameter of the neighboring subsystem of the same type parameter, as the losses within the distribution elements were neglected. Therefore, the reader can infer input or output parameter missing in Figure 12 from the corresponding output or input parameters, respectively. For instance, information on the power converter input power can be inferred from the battery output power plot in the figure.

It can be seen from Figure 12 that power requirements from each PG&D is different. This is because each subsystem has its own inefficiency. The plots in Figure 12 is given for individual subsystems. Since there are only one battery and one power converter, the power requirement from them are greater than the electric motors. That's why the current at the input ports of the electric motors are significantly less than the outgoing battery current. This effect can also be seen in the voltage variations, where the battery voltage

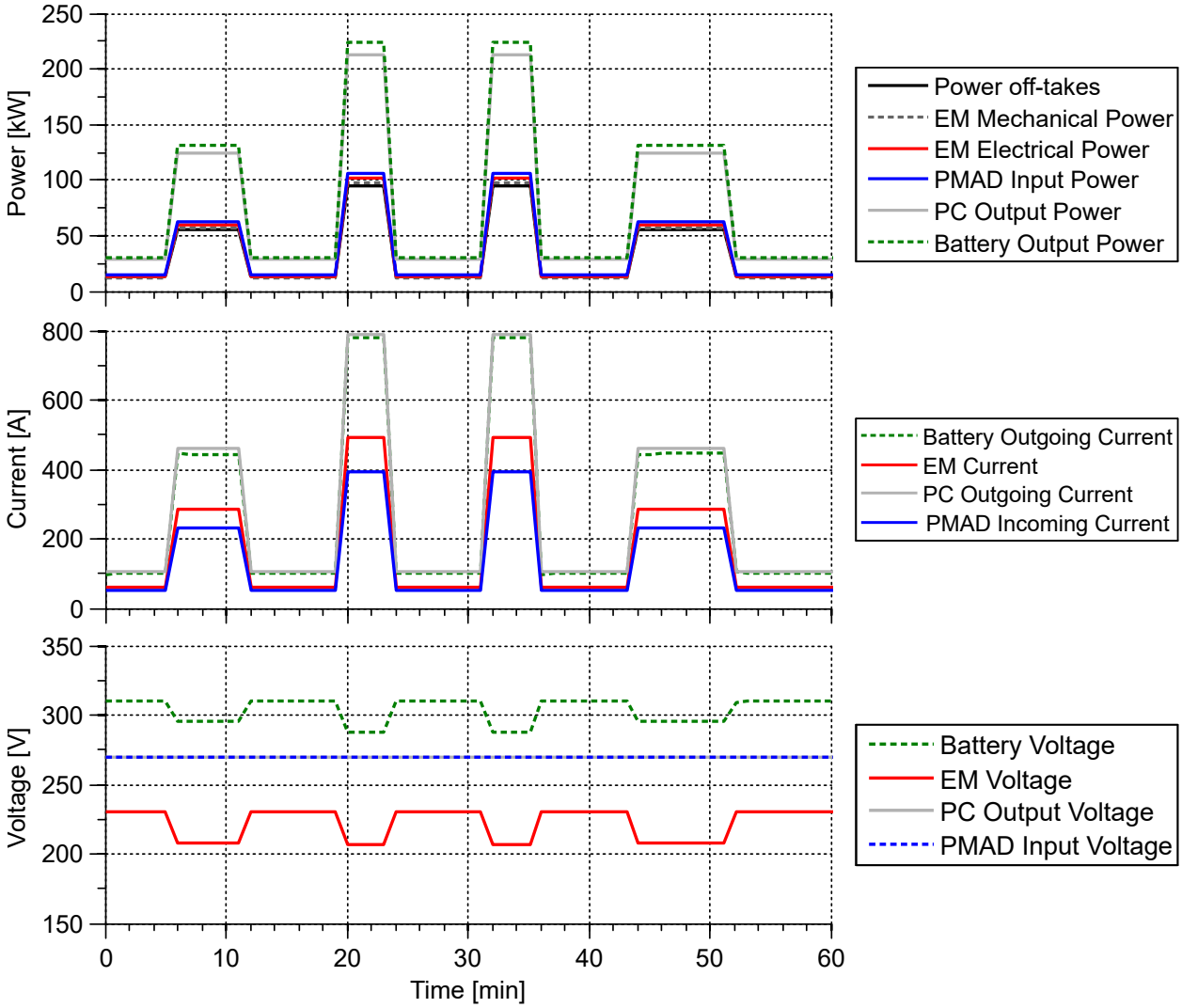

Figure 12. PG&D subsystem input and output parameters through time under the varying power requirement

is much greater than the electric motor voltage. The power converter voltage is constant at 270 V, which was chosen to be the system voltage.

The part *(a)* of the Figure 13 shows the battery state of charge decreasing nonlinearly from 100% (fully charged battery) to about 20% (the preset minimum limit). The electric motor efficiency variation under different power requirements can be seen in part *(b)* of the same figure. The electric motor characteristics given in Table 4 results in a motor efficiency as low as 86% and as high as 96%. This plot can be very helpful to choose the right electric motor characteristics by determining under which operating conditions (i.e. power setting) the highest motor efficiency is sought.

There are numerous aspects that the developed models have to offer. Here, we shall give an example to how a system architect can make use of the results given in Figure 12, but the analysis can be extended to many other architectural design choices.

Under the given conditions, the highest amount of current is about 790 A, seen at the output port of the power converter. The battery current is also very high, with a peak of 781 A. Pacelab SysArc can calculate the weight of the electric cables between the subsystem components Pacelab SysArc through their length and linear density. The linear density is dictated by the chosen cable type. Pacelab SysArc also has a library of cable types along with information on maximum current allowance and linear density for each cable type. The electric cable types between the subsystems were chosen according to the maximum current allowance

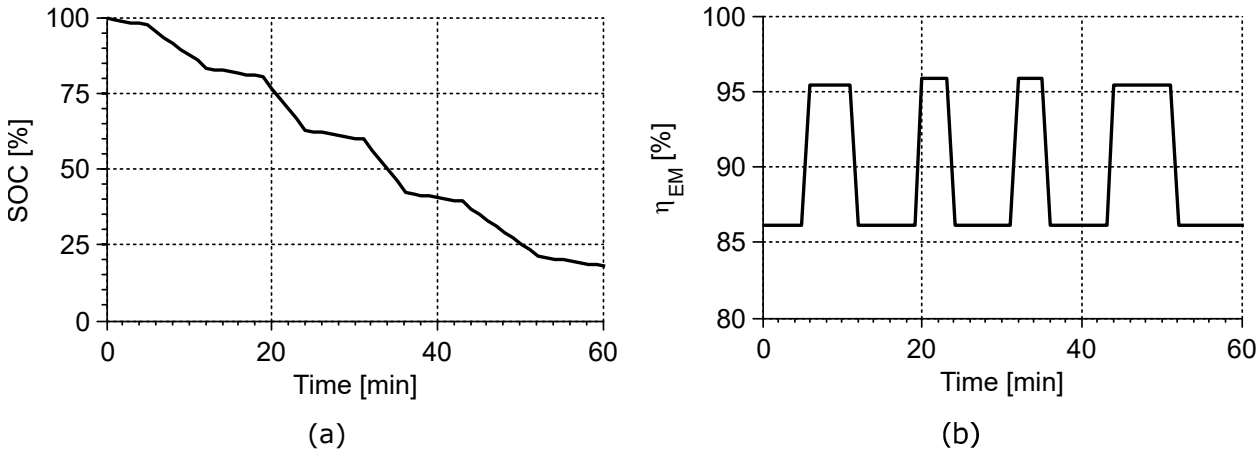

Figure 13. (a) Battery state of charge, (b) Electric motor efficiency

and the highest current obtained during the analysis, as listed in Table 5. The cable lengths (and weights) between the power converter and motor, the generator and bus, and the bus and load were given for a single branch; and thus they must be multiplied by 2 in order to calculate the total cable lengths (and weights). The total cable weight for this configuration was found as 40 kg. However, in the upcoming analysis, percentage changes will be taken into account rather than the absolute values since the subsystems were located rather arbitrarily.

Table 5. Electric cable characteristics for a system voltage of 270 V

Location:	Battery - Converter	Converter - Motor	Generator - Bus	Bus - Load
Type:	AWG 5/0	AWG 1/0	AWG 7	AWG 7
Length [m]:	2.81	18.56 (x2)	40.55 (x2)	30.96 (x2)
Linear Density [kg/m]:	1.31	0.53	0.12	0.12
Cable Weight [kg]:	3.69	9.93 (x2)	4.66 (x2)	3.56 (x2)

If the battery and power converter in this example were replaced farther apart than each other and the rest of the subsystems, then these high amounts of current might have resulted in significantly heavy electric cables. In such cases, subsystems with different characteristics can be chosen in order to decrease the current. One architecture choice that can be altered is the system voltage which was previously set to 270 V. The selection of the system voltage depends on many considerations, including the operating voltage of other subsystems, converter efficiencies, cable weights, etc. If it is assumed that the power converter and PMAD units can be kept at the same efficiency when the system voltage is increased, then the battery current would decrease proportionally under the same power requirements. Figure 14 demonstrates the resulting current and voltage changes when the system voltage is doubled from 270 V to 540 V and the rest of the subsystem characteristics are kept constant. The power variations remain the same as given in Figure 12 and therefore was not shown in Figure 14 for the second time.

It can be seen in Figure 14 that by doubling the system voltage, the battery and power converter outgoing current values were decreased significantly, with a peak of 394 A at the power converter output. Although the incoming current to the PMAD also dropped, the electric motor current and voltage did not change. This is due to the fact that the motor current and voltage are proportional to the motor torque and angular speed respectively, and since neither the torque nor the speed were changed, motor current and voltage did not change either.

The reduction of battery and power converter outgoing currents allowed for lighter cables between these ports, as it can be seen in Table 6. By changing the cable types between the battery and power converter, and the power converter and motors, the total cable weight was reduced to 24.5 kg. This is a cable weight savings of 38.7% over the previous architecture with 270 V of system voltage. It should be kept in mind

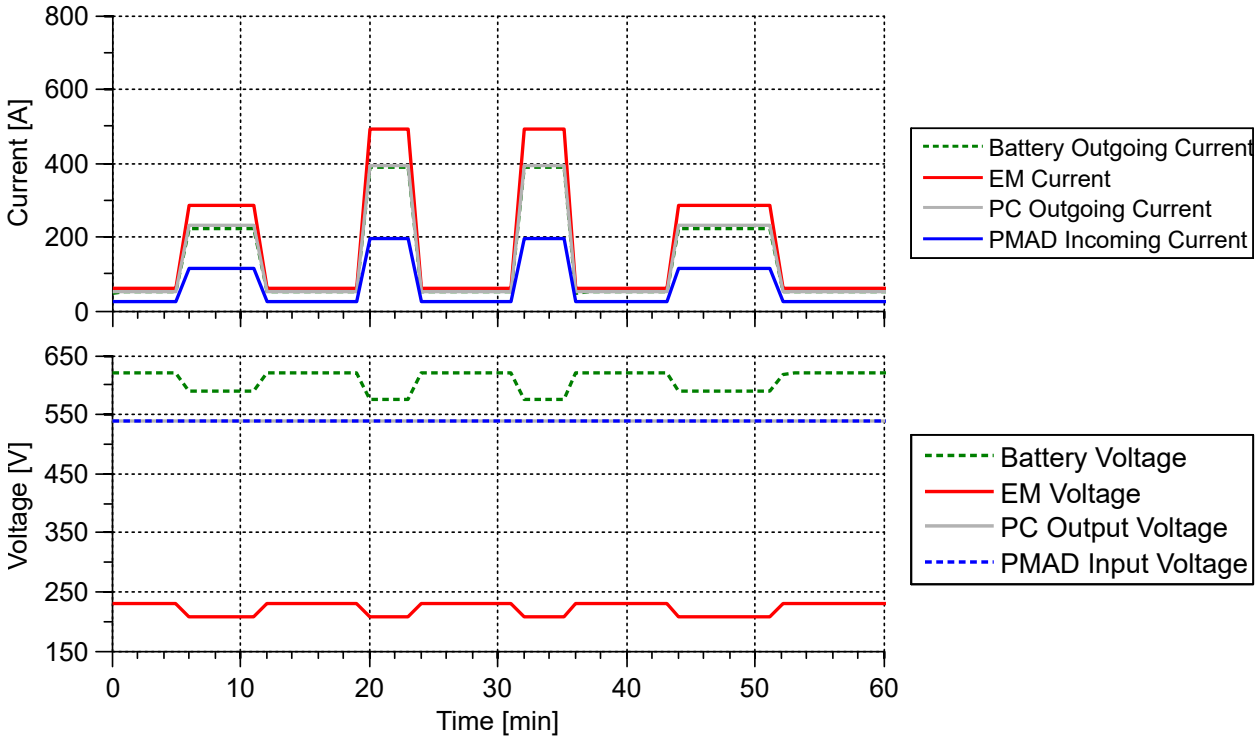

Figure 14. PG&D subsystem input and output parameters through time under the varying power requirement

that the converter efficiency was kept constant during this study. In reality, as the difference between the input and output power (or voltage) values increase, the converter efficiency will most likely decrease. This might result in a heavier converter and therefore change the results. This change can be simulated using the developed models by varying the power converter efficiency accordingly.

Table 6. Electric cable characteristics after the system voltage was increased to 540 V

Location:	Battery - Converter	Converter - Motor	Generator - Bus	Bus - Load
Type:	AWG 1/0	AWG 5	AWG 7	AWG 7
Length [m]:	2.81	18.56 (x2)	40.55 (x2)	30.96 (x2)
Linear Density [kg/m]:	0.53	0.18	0.12	0.12
Cable Weight [kg]:	1.50	3.29 (x2)	4.66 (x2)	3.56 (x2)

Although a simple application case was demonstrated in this section, the models can be used to simulate many other scenarios and to explore the design space under different conditions and performance characteristics.

VI. Conclusion and Future Work

The main purpose of this work was to develop easy-to-use, physics-based and parametric PG&D subsystem models for rapid and low cost analyses at conceptual aircraft design stage. To this end, four main PG&D subsystem components (i.e. rechargeable battery, power converter, electric motor and propeller speed reduction unit) were identified. A comprehensive literature survey was made to find suitable physics-based models for architecture design studies at early design stages. The chosen models were developed and adapted to suit the purpose of the work.

The emphasis was made on the capturing the dynamic behavior of rechargeable batteries under varying power requirements. A flexible battery model was developed to represent future capabilities. The battery

level requirements were translated into cell level characteristics to enable more informed design decisions.

The modeling and simulation environment to build the models and carry on the analysis was chosen to be Pacelab SysArc, a system architecture design tool that allows building, analyzing and optimizing system and subsystem architectures. The sizing methods for each subsystem were explained in detail. Then, a methodology to integrate the models was presented. The information propagation between the models that allows sizing each components simultaneously was also described.

The developed PG&D subsystem models also facilitate architecture design space exploration studies. A sample application was provided within a parallel hybrid-electric architecture. In this example, the Dornier 328 was chosen as the baseline aircraft. Then, PG&D subsystems were placed inside the aircraft such that a single battery pack fed two electric motors connected to the two propellers. Two electric loads were also connected to the motors via generators. These loads were used to represent varying power off-takes throughout a flight segment by assigning a specific power schedule with three different power settings. After all the PG&D subsystems were automatically sized, the subsystem behaviors under these varying power requirements were monitored.

It was shown that the power, current and voltage at input and output ports of each subsystem model could be easily tracked and the information could be used to make further design decisions. An example was given where the system voltage was doubled in order to reduce the cable weights. By doing so, the overall cable weight for the electric propulsion branch of the given architecture was decreased by 38.7%. Although the absolute values of the cable weights were rather insignificant compared to the baseline aircraft weight, the high value of the relative weight change shows that they might make an important difference under larger power requirements and different architectures. In fact, the relative change in terms of cable weights can be very significant when it comes to architecture evaluations. It must also be noted that in this example, such a change was obtained by changing a single parameter value, demonstrating the fact that even small changes can make a big impact on the overall architecture.

The sample application provided here can be extended to much complex problems. The parametric nature of the models enables sensitivity analysis and technology projections. Moreover, with the help of these models, the couplings and interrelations between these subsystem components and the vehicle performance can be revealed at early design stages. Such a study was carried on by the authors using these models within a parallel hybrid electric architecture, where the authors performed sensitivity analysis and architecture comparisons.[21]

Although the PG&D subsystem models were developed at a rather detailed level, there is still more to add to this work. Although the volume of each component can be provided by the user, a volumetric specific energy or power must also be defined for each subsystem model. Hence, the modeling and sizing of the subsystems will be extended to include volumetric considerations in the future. Furhermore, the effects of thermodynamic losses and cooling will also be implemented. Finally, the battery model will be improved to have a charging capability.

References

[1]IATA, "IATA Technology Roadmap," June 2013.

[2]National Academies of Sciences, Engineering, and Medicine, *Commercial Aircraft Propulsion and Energy Systems Research: Reducing Global Carbon Emissions*, The National Academies Press, Washington DC, 2016.

[3]Hornung, M., Isikveren, A. T., Cole, M., and Sizmann, A., "Ce-Liner Case Study for eMobility in Air Transportation," AIAA, Los Angeles, CA, August 12-14 2013.

[4]Bradley, M. K. and Droney, C. K., "Subsonic Ultra Green Aircraft Research: Phase II Volume II Hybrid Electric Design Exploration," Tech. rep., Boeing Research and Technology, Huntington Beach, California, April 2015.

[5]Madavan, N. K., Del Rosario, R., and Jankovsky, A. L., "Hybrid-Electric and Distributed Propulsion Technologies for Large Commercial Transports: A NASA Perspective," Special Session on Future Electric Aircraft - Systems, IEEE, Montreal, Canada, 20-24 Sep. 2015.

[6]Roskam, J., *Airplane Design Part V - Component Weight Estimation*, Design Analysis and Research Corporation, Kansas, 1999.

[7]Raymer, D. P., *Aircraft Design: A Conceptual Approach*, AIAA Education Series, AIAA, Virginia, 5th ed., 2012.

[8]Mattingly, J. D., Heiser, W. H., and Pratt, D. T., *Aircraft Engine Design*, AIAA Education Series, AIAA, 2nd ed., 2002.

[9]Cinar, G., Emeneth, M., and Mavris, D. N., "A Methodology for Sizing and Analysis of Electric Propulsion Subsystems for Unmanned Aerial Vehicles," 54th AIAA Aerospace Sciences Meeting, AIAA, San Diego, CA, January 4-8 2016.

[10]Lowry, J. and Larminie, J., *Electric Vehicle Technology Explained*, John Wiley & Sons, 2nd ed., June 2012.

[11]Chen, M. and Rincon-Mora, G. A., "Accurate Electrical Battery Model Capable of Predicting Runtime and IV Performance," *IEEE Transactions on Energy Conversion*, Vol. 21, No. 2, June 2006, pp. 504–511.

[12]Ramadesigan, V., Northrop, P. W. C., De, S., Santhanagopalan, S., Braatz, R. D., and Subramanian, V. R., "Modeling and Simulation of Lithium-Ion Batteries from a Systems Engineering Perspective," *Journal of The Electrochemical Society*, Vol. 159, No. 3, January 2012, pp. R31–R45.

[13]Jongerden, M. R. and Haverkort, B. R., "Which battery model to use?" *IET Software*, Vol. 3, No. 6, December 2009, pp. 445–457.

[14]He, H., Xiong, R., and Fan, J., "Evaluation of Lithium-Ion Battery Equivalent Circuit Models for State of Charge Estimation by an Experimental Approach," *Energies*, Vol. 4, March 2011, pp. 582–598.

[15]Tremblay, O. and Dessaint, L. A., "Experimental validation of a battery dynamic model for EV applications," *World Electric Vehicle Journal*, Vol. 3, No. 1, May 2009, pp. 1–10.

[16]Emadi, A., Young, J. L., and Kaushik, R., "Power electronics and motor drives in electric, hybrid electric, and plug-in hybrid electric vehicles," *IEEE Transactions on Industrial Electronics*, Vol. 55, No. 6, Jun 2008, pp. 2237–2245.

[17]Siemens AG, "World-record Electric Motor For Aircraft," [company website], Mar. 2015, URL: http://www.siemens.com/press/en/feature/2015/corporate/2015-03-electromotor.php?content[]=Corp [cited on 13 Sep. 2015].

[18]Metcalf, K., "Power Management and Distribution (PMAD) Model Development," Tech. Rep. NASA/CR2011-217268, Boeing Corporation, Canoga Park, CA, November 2011.

[19]Hendricks, E. and Tong, M., "Performance and Weight Estimates for an Advanced Open Rotor Engine," 48th AIAA/ASME/SAE/ASEE Joint Propulsion Conference & Exhibit, Joint Propulsion Conferences, AIAA, Atlanta, GA, 30 July 1 Aug 2012.

[20]Miranda, D., Costa, C., and Lanceros-Mendez, S., "Lithium ion rechargeable batteries: State of the art and future needs of microscopic theoretical models and simulations," *Journal of Electroanalytical Chemistry*, Vol. 739, 2015, pp. 97–110.

[21]Cinar, G., Mavris, D. N., Emeneth, M., Schneegans, A., Riediger, C., Fefermann, Y., and Isikveren, A., "Sizing, Integration and Performance Evaluation of Hybrid Electric Propulsion Subsystem Architectures," 55th AIAA Aerospace Sciences Meeting, AIAA, Grapevine, TX, January 9-13 2017.

[22]328 Design GmbH, "Dornier 328-100 TP," Company website, August 2013, URL: http://328.eu/wp-content/uploads/2013/06/328-100-turboprop.pdf [cited 22 Nov 2016].